COHERENT RADAR IMAGING USING UNSYNCHRONIZED DISTRIBUTED ANTENNAS

Muhammad Asad Lodhi[*]

Rutgers University
Dept. of Elec. and Comp. Engineering
masad.lodhi@rutgers.edu

Hassan Mansour, Petros T. Boufounos[†]

Mitsubishi Electric Research Laboratories
{*mansour,petrosb*}@merl.com

ABSTRACT

In this paper we develop an optimization-based solution to the problem of distributed radar imaging using antennas with asynchronous clocks. In particular, we consider a distributed radar imaging MIMO system observing a sparse scene under an unknown, but bounded, delay between the transmitter and receiver clocks. Most existing approaches pose the problem as the recovery of a phase shift, leading to non-convex formulations. Instead, inspired by recent work in blind deconvolution, we exploit the realization that synchronization errors in the received data can be modeled as a convolution with an unknown 1-sparse delay signal to be estimated in addition to the image. Thus, we formulate a convex optimization problem that simultaneously recovers all the pair-wise drifts between transmit/receive pairs, as well as the sparse scene being imaged. We verify the validity and performance of our proposed model and recovery method through numerical simulations on synthetic data.

Index Terms— radar autofocus, blind deconvolution, time synchronization, convex programming

1. INTRODUCTION

Distributed radar arrays are essential for high resolution radar imaging as they allow for a large overall aperture by combining information from several spatially distributed radar antennas with small individual apertures. Furthermore, these arrays also enable a flexible mobile platform that is tolerant to sensor failures and admits low maintenance costs [1–4]. However, geographical distribution of an array introduces data coherence problems due to ambiguities in the position of the antennas and difficulties in precisely synchronizing the antenna clocks.

Typically, both of these issues are often modeled as phase errors in the received data [5–10]. Indeed, a time delay introduced due to clock drift is equivalent to a phase shift that is linear in frequency. Similarly, a position error introduces time shifts in the reflections depending on the geometry of the targets in the image, which can also be modeled as combinations of phase shifts linear in frequency. More detailed discussion of this model can be found in [11] and references within. Most of the literature attempts to estimate and correct the phase errors in the data, in order to apply coherent imaging techniques on the corrected data.

A common issue with those techniques is that the estimation of the phase error is not straightforward due to the non-linearity of the resulting formulation [12–14] and the additional complication of phase wrapping. Furthermore, typical phase models in the literature, such as subspace restrictions, often under-perform because they fail to capture the true nature of the error.

Instead, our approach explicitly models the time uncertainty as an unknown time delay in the recorded data, i.e., a convolution with a delay operator. Thus, we can accurately model time delays due to clock drifts, as opposed to arbitrary phase errors. Our formulation results in a convex optimization problem, the solution to which simultaneously provides both the radar image and the pairwise clock drifts between transmitter/receiver pairs. Our solution provides the resolution benefits of coherent imaging, even if the measurements are not coherent.

The work in this paper is in many ways similar to our earlier work in [11], in which we explicitly model position ambiguities on the distributed antennas but assume perfect synchronization. Our line of work in this area is inspired by earlier works in sparse blind deconvolution [12–15], that use lifting or alternating minimization to solve the resulting bilinear problem. Both our prior work and this paper demonstrate that proper use of sparsity can provide accurate models of the errors encountered in distributed array problems. However, there is a key difference. The bi-linear formulation in [11] results in a non-convex problem that is solved with an alternating minimization. Although the problem can in principle be lifted to a higher space and convexified, the resulting optimization becomes prohibitively expensive. In contrast, the nature of timing errors that we explore in this paper, enables a tractable convex formulation without resorting to lifting. Thus, we can provide a FISTA [16] based procedure to recover the radar scene. Of course, a combination of the two approaches, which corrects both for position and synchronization errors is possible, but we defer it to a future publication.

We should note that another option in handling these phase errors, at the cost of decreased performance, is to assume they cannot be recovered and develop algorithms that are robust to arbitrary phase errors. These approaches are collectively known as incoherent imaging [3, 17, 18] and typically suffer from lower resolution and worse reconstruction performance. This is not an approach we consider in this paper, because of its poor reconstruction accuracy.

The next section of this paper describes the problems and its formulation. Section 3 provides a solution model for our formulation and our FISTA-based algorithm to obtain the solution. Simulation-based numerical results that validate our approach are presented in Section 4. Section 5 discusses our results and concludes.

2. PROBLEM FORMULATION

In this section we present a convex formulation of the radar autofocus problem suffering from asynchronous clocks.

[*]ML did this work while an intern at MERL, supported by NSF INTERN Supplemental Funding for NSF Award # CCSS-1509260

[†]HM and PB are exclusively supported by MERL

2.1. System Model

We consider a two-dimensional radar scene of size $N = N_x \times N_y$ containing K static targets, where N_x and N_y represent the horizontal and vertical dimensions, respectively. We also consider a set of antennas, some of which may act as transmitters only, some as receivers only, and some as both. We assume that transmitters transmit one at a time, i.e., the received reflection in any receiver at any point in time is only due to one transmitter transmitting. For any single transmission, multiple receivers receive the reflections from the scene. We use $m = 1, \ldots, M$ to index all possible combinations of active transmitter/receiver pairs during the system operation.

To observe the scene, a transmitting antenna emits a pulse $p(t)$ with frequency spectrum $P(\omega)$, where ω is the angular frequency corresponding to the actual frequency $f \in \mathcal{B}$ and the bandwidth of the transmitted pulse is $|\mathcal{B}| = F$. The pulse propagates through the scene before it is reflected back to a receiving antenna that measures the signal

$$r_m(t) = \sum_{k=1}^{K} x_k p(t) * a_m^k(t), \tag{1}$$

where x_k denotes the reflectivity of target k, a_m^k denotes the impulse response of the channel that describes the propagation of the reflected pulse from the transmitter to the target k and back to the receiver, for the transmitter/receiver pair m, and $*$ denotes the convolution operation. Typically for radar in free space, a_m^k comprises of a delay and attenuation depending on the round-trip distance of the pulse to the target and back to the receiver.

The signal model in equation (1) assumes that the clocks controlling the transmitting and receiving antennas are synchronized. If the transmitter/receiver pairs are not synchronized, then the received signal will be delayed according to the relative advance of the receiver clock compared to the transmitter clock (or advanced, if the receiver clock is delayed). Using ϵ_m to denote the relative time advance of the receiver, the received signal in the receiver's clock is equal to

$$\begin{aligned} y_m(t) &= \textstyle\sum_{k=1}^{K} x_k p(t - \epsilon_m) * a_m^k(t), \\ &= r_m(t) * \delta(t - \epsilon_m), \end{aligned} \tag{2}$$

where $\delta(t - \epsilon_m)$ is the impulse response representing the relative delay of the data in the receiver's clock, due to the clock mismatch. Equivalently, we can advance both sides of (2) by ϵ_m, to obtain

$$y_m(t) * \delta(t + \epsilon_m) = r_m(t) = \sum_{k=1}^{K} x_k p(t) * a_m^k(t). \tag{3}$$

In frequency, this is equivalent to

$$Y_m(\omega) e^{j\omega\epsilon_m} = R(\omega) = \sum_{k=1}^{K} P(\omega) A_m^k(\omega) x_k. \tag{4}$$

2.2. Model Discretization

To discretize in space, we use $\mathbf{x}$ to denote the reflectivity of all points in the scene, under a pre-determined, sufficiently fine grid. Assuming no synchronization errors, the frequency-domain received data for each transmitter/receiver pair can be represented as

$$\mathbf{r}_m = \mathbf{A}_m \mathbf{x}, \tag{5}$$

where the matrix $\mathbf{A}_m$ incorporates, in frequency, the transmitted pulse $P(w)$ and the channel response $A_m^k(\omega)$.

Using $Z(\omega) = e^{j\omega\epsilon_m}$ to denote the advance $z(t) = \delta(t + \epsilon_m)$ in the frequency domain, the data in the receiver's clock satisfy

$$\mathbf{D}_{\mathbf{y}_m} \mathbf{F} \mathbf{z}_m = \mathbf{A}_m \mathbf{x}, \tag{6}$$

where, $\mathbf{y}_m$ is the frequency-domain received data, $\mathbf{z}_m$ is the time domain advance, F is the Fourier transform matrix, and $\mathbf{F}\mathbf{z}_m$ is the Fourier transform of $\mathbf{z}_m$, i.e., the frequency-domain representation of the advance, and $\mathbf{D}_{\mathbf{y}_m}$ is a diagonal operator with $\mathbf{y}_m$ in the diagonal.

Assuming that $\mathbf{y}_m$ does not have any frequency content equal to zero, (6) can be written as

$$\mathbf{F}\mathbf{z}_m = \mathbf{D}_{\mathbf{y}_m}^{-1} \mathbf{A}_m \mathbf{x}, \tag{7}$$

$$\Rightarrow [\mathbf{D}_{\mathbf{y}_m}^{-1} \mathbf{A}_m \quad -\mathbf{F}] \begin{bmatrix} \mathbf{x} \\ \mathbf{z}_m \end{bmatrix} = \mathbf{0}, \tag{8}$$

where $\mathbf{0}$ is a zero vector of appropriate dimension, and, since $\mathbf{D}_{\mathbf{y}_m}$ is diagonal, it's inverse $\mathbf{D}_{\mathbf{y}_m}^{-1}$ is simply the element-wise inverse of the diagonal. In other words, assuming no noise, the vector $[\mathbf{x} \quad \mathbf{z}_m]^T$ is in the nullspace of $[\mathbf{D}_{\mathbf{y}_m}^{-1} \mathbf{A}_m \quad -\mathbf{F}]$. The equivalent model in the presence of noise, is

$$[\mathbf{D}_{\mathbf{y}_m}^{-1} \mathbf{A}_m \quad -\mathbf{F}] \begin{bmatrix} \mathbf{x} \\ \mathbf{z}_m \end{bmatrix} = \mathbf{n}, \tag{9}$$

where $\mathbf{n}$ represents additive noise in the frequency domain.

Our goal is to recover $\mathbf{x}$ and $\mathbf{z}$ under the constraints that $\mathbf{x}$ is a sparse scene and $\mathbf{z}$ is a delay, i.e., a 1-sparse signal.

3. SYNCHRONIZATION AND SCENE RECOVERY

3.1. Solution Model and Constraints

With measurements from all the transmitter-receiver pairs, the overall system of equations takes the following form:

$$\begin{bmatrix} \widetilde{\mathbf{A}}_1 & -\mathbf{F} & \Theta & \Theta & \cdots & \Theta \\ \widetilde{\mathbf{A}}_2 & \Theta & -\mathbf{F} & \Theta & \cdots & \Theta \\ \vdots & \vdots & \vdots & \vdots & \ddots & \vdots \\ \widetilde{\mathbf{A}}_M & \Theta & \Theta & \Theta & \cdots & -\mathbf{F} \end{bmatrix} \begin{bmatrix} \mathbf{x} \\ \mathbf{z}_1 \\ \mathbf{z}_2 \\ \vdots \\ \mathbf{z}_M \end{bmatrix} = \begin{bmatrix} \mathbf{n}_1 \\ \mathbf{n}_2 \\ \vdots \\ \mathbf{n}_M \end{bmatrix} \tag{10}$$

where $\widetilde{\mathbf{A}}_m = \mathbf{D}_{\mathbf{y}_m}^{-1} \mathbf{A}_m$, Θ is an $F \times F$ matrix of all zeros, and F is the number of frequencies used in the discretized system.

The true radar scene and the true time shifts lie in the nullspace of the matrix in the left-hand side of (10), which, however, might not be unique. To reduce the ambiguity and to avoid trivial solutions, such as all zeros, we need to introduce additional constraints on the feasible set. Since the delay operator $\mathbf{z}_m$ is a simple time shift, we constrain it to be non-negative. In addition, by design, $\mathbf{z}_m$ is a delay and, therefore, 1-sparse for each m. Similarly, $\mathbf{x}$ is sparse by assumption.

We also impose a scale constraint on both unknowns ($\mathbf{x}$ and $\mathbf{z}_m$). A soft scale constraint on the scene reflectivity $\mathbf{x}$ helps avoid trivial solutions by ensuring that the sum of the entries in $\mathbf{x}$ moves away from zero. In particular, the scale constraint on $\mathbf{x}$ is achieved by including a regularized least squares penalty that forces the sum of entries in $\mathbf{x}$ to be equal to a nonzero constant c. The value of c may be estimated by solving an initial inverse problem to recover $\mathbf{x}$ while ignoring the synchronization ambiguity and setting c to be equal to

Algorithm 1: FISTA for distributed radar phase-synchronization

Input: measurements $\{\mathbf{y}_m\}_{m=1}^M$, measurement matrices $\{\mathbf{A}_m\}_{m=1}^M$, Lipschitz constant α, and regularization parameters $\lambda_x\ \lambda_z\ \gamma$

Initialization: Initial estimate $\mathbf{w}^0 = \mathbf{u}^0$, $t^0 = 1$

1: **while** stopping criteria unsatisfied **do**
2: $\quad \mathbf{v}^j \leftarrow \mathbf{w}^{j-1} + \alpha \mathbf{B}^H(\mathbf{b} - \mathbf{B}\mathbf{w}^{j-1})$
3: $\quad \bar{\mathbf{u}}^j \leftarrow \mathcal{T}(\mathbf{v}^j, \alpha\lambda)$
4: $\quad \mathbf{u}^j \leftarrow \mathbf{P}_{\mathbb{R}_+}(\bar{\mathbf{u}}^j)$
5: $\quad t^j \leftarrow \frac{1+\sqrt{1+4(t^{j-1})^2}}{2}$
6: $\quad \mathbf{w}^j \leftarrow \mathbf{u}^j + \frac{t^{j-1}-1}{t^j}(\mathbf{u}^j - \mathbf{u}^{j-1})$
7: **end while**

Output: Final estimate $\mathbf{w}^j$

the sum of entries of the resulting reflectivity image. The scale constraints for the time shifts $\mathbf{z}_m$, on the other hand, are imposed as a hard constraint: $\mathbf{1}^T\mathbf{z}_m = 1$ for each m.

Combining all constraints and priors, we obtain the following sparse recovery problem:

$$\underset{\mathbf{x},\{\mathbf{z}_m\}_{m=1}^M}{\text{minimize}} \quad \lambda_x \|\mathbf{x}\|_1 + \lambda_z \sum_{m=1}^{M} \|\mathbf{z}_m\|_1 + \left\| \begin{bmatrix} \widetilde{\mathbf{A}}_1 & -\mathbf{F} & \Theta & \Theta & \cdots & \Theta \\ \widetilde{\mathbf{A}}_2 & \Theta & -\mathbf{F} & \Theta & \cdots & \Theta \\ \vdots & \vdots & \vdots & \vdots & \ddots & \vdots \\ \widetilde{\mathbf{A}}_M & \Theta & \Theta & \Theta & \cdots & -\mathbf{F} \\ \gamma\mathbf{1}_N^T & \mathbf{0}_P^T & \mathbf{0}_P^T & \mathbf{0}_P^T & \cdots & \mathbf{0}_P^T \end{bmatrix} \begin{bmatrix} \mathbf{x} \\ \mathbf{z}_1 \\ \mathbf{z}_2 \\ \vdots \\ \mathbf{z}_M \end{bmatrix} - \begin{bmatrix} 0 \\ 0 \\ \vdots \\ 0 \\ \gamma c \end{bmatrix} \right\|_2^2$$

$$\text{subject to:} \quad \mathbf{x} \geq \mathbf{0}_N\ ,\ \mathbf{z}_m \geq \mathbf{0}_P\ ,\ \mathbf{1}^T\mathbf{z}_m = 1\ ,\ \forall m \qquad (11)$$

where $\mathbf{1}$ and $\mathbf{0}$ are vectors of all ones and zeros of appropriate lengths.

3.2. FISTA-based Recovery Algorithm

Since the problem posed in (11) is a convex sparse recovery problem, we propose a FISTA inspired algorithm to find the solution. To this end, let us first define the following variables:

$$\mathbf{w} = \begin{bmatrix} \mathbf{x} \\ \mathbf{z}_1 \\ \mathbf{z}_2 \\ \vdots \\ \mathbf{z}_M \end{bmatrix},\ \mathbf{b} = \begin{bmatrix} 0 \\ 0 \\ \vdots \\ 0 \\ \gamma 1 \end{bmatrix},\ \lambda = \begin{bmatrix} \lambda_x\mathbf{1}_N \\ \lambda_z\mathbf{1}_P \\ \lambda_z\mathbf{1}_P \\ \vdots \\ \lambda_z\mathbf{1}_P \end{bmatrix},\ \text{and}$$

$$\mathbf{B} = \begin{bmatrix} \widetilde{\mathbf{A}}_1 & -\mathbf{F} & \Theta & \Theta & \cdots & \Theta \\ \widetilde{\mathbf{A}}_2 & \Theta & -\mathbf{F} & \Theta & \cdots & \Theta \\ \vdots & \vdots & \vdots & \vdots & \ddots & \vdots \\ \widetilde{\mathbf{A}}_M & \Theta & \Theta & \Theta & \cdots & -\mathbf{F} \\ \gamma\mathbf{1}^T & \mathbf{0}^T & \mathbf{0}^T & \mathbf{0}^T & \cdots & \mathbf{0}^T \end{bmatrix}. \qquad (12)$$

With these variables, the algorithm for blind deconvolution is presented in Alg. 1. Before starting the algorithm, the estimate $\mathbf{w}^0$ is initialized with $\mathbf{x}^0 = \mathbf{0}_N$ and all $\mathbf{z}_m^0 = \mathbf{z}^0$, where $\mathbf{z}^0$ is the time-domain Dirac delta and corresponds to no time ambiguity in the measurements. At step 3 of the algorithm, $\mathcal{T}(\cdot)$ represents the element-wise soft-thresholding operator defined as:

$$\mathcal{T}(x,\lambda) = \begin{cases} \text{sign}(x_i)\cdot\big(|x_i| - \lambda\big), & \text{if } |x_i| \geq \lambda \\ 0, & \text{otherwise.} \end{cases} \qquad (13)$$

Furthermore, at step 4, $\mathbf{P}_{\mathbb{R}_+}(\cdot)$ represents the projection of the $\mathbf{z}_m$ components of $\bar{\mathbf{u}}$ onto the non-negative real orthant, followed by the normalization of all $\mathbf{z}_m^j$'s to strictly impose the scale constraint $\mathbf{1}^T\mathbf{z}_m = 1$. We now evaluate the performance of our modified FISTA approach on synthetic data.

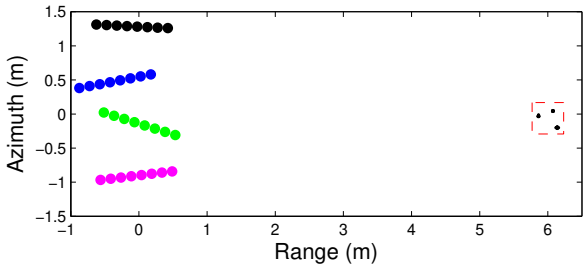

Fig. 1. The synthetic distributed radar system in our synthetic data. The colored round dots represent antennas in the four distributed array. The red square represents the radar scene being imaged.

4. NUMERICAL EXPERIMENTS

To evaluate the performance of our proposed method, we run experiments for a synthetic radar scene with three targets as shown in Fig. 1. The measurements are obtained through four wideband distributed antenna arrays with 8 antennas on each array. The first antenna array acts as both transmitter and receiver, whereas the other three act only as receivers. The system bandwidth is 6GHz, centered at 6GHz, and the received signals are sampled at the Nyquist rate. The simulations are performed in the time domain.

The measurements acquired from the first array have no time mismatch since the same array is used for both transmission and signal acquisition. For the remaining three arrays a time mismatch (advance or delay) of $T_{\max}$ is allowed. The measurements are corrupted with white Gaussian noise having a peak signal-to-noise ratio (PSNR) of 30dB after matched filtering with the transmitted pulse. The radar scene recovered through the proposed algorithm is shown in Fig. 2, along with the ground truth and reconstructions from sparse recovery with correct and incorrect antenna positions. We run our algorithm with λ_x and λ_z equal to 200 for $T_{\max} = 5$ time samples. The advantage of our proposed method is evident from the comparison, and one can see that our method reconstructs the radar scene correctly up to a global shift ambiguity.

To highlight the effect of noise in the observations on the recovery performance, we also compare our proposed approach against the sparse recovery algorithm with incorrect positions. We run experiments for varying PSNR levels and for maximum time errors $T_{\max}$ of 5 and 20 time samples. We generate five different spatial realizations of "three targets" in the scene each with different time ambiguities. We then generate receiver operating characteristic (ROC) curves for both approaches at the varying PSNR levels ranging from 8dB to 30dB. It can be seen from Fig. 3 that our proposed approach outperforms sparse recovery with incorrect positions at all noise levels.

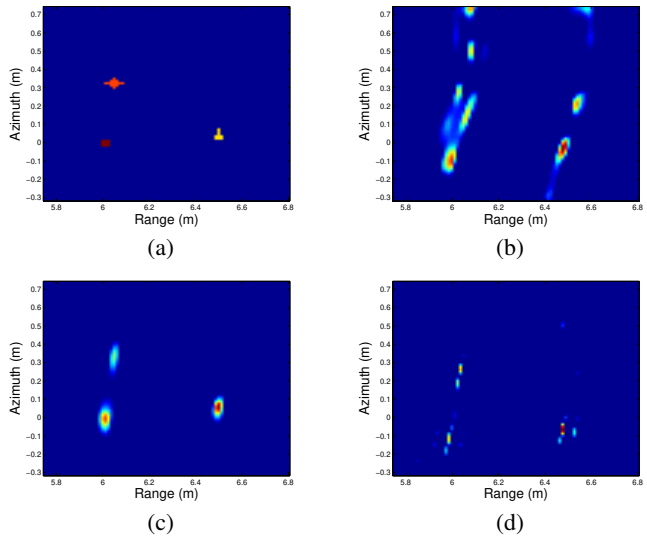

Fig. 2. Figure (a) shows the true reflectivity of the target scene. Figures (b) and (c) show the reconstructed scenes with unknown and known time mismatch, respectively. Figure (d) shows the reconstructed scene obtained through the proposed approach that recovers the scene as well as the time mismatch.

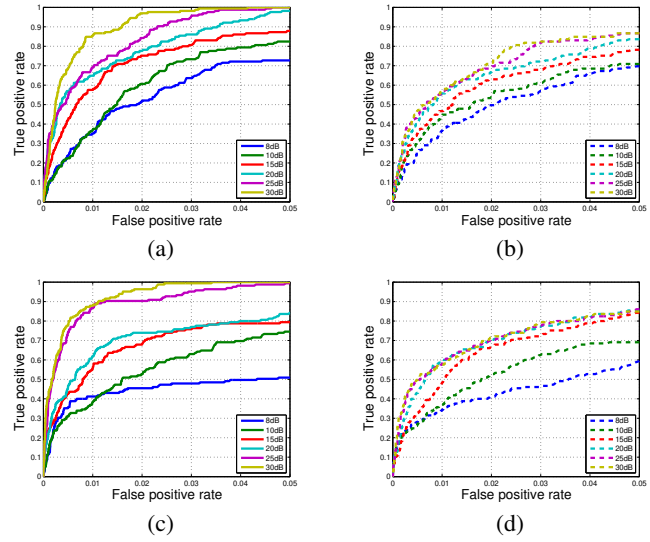

Fig. 3. The top row presents the ROC curves for (a) the proposed algorithm and (b) sparse recovery algorithm with time errors for a maximum time mismatch of 5 time periods. The bottom row shows the same ROC curves for a maximum time mismatch 20 time periods.

5. CONCLUSION

In this paper we demonstrate that appropriate modeling of the clock asynchrony in distributed radar systems provides the ability to perform coherent imaging, despite the significant phase errors in the acquired data. The key realization is that asynchronous clocks manifest as unknown delays or advances in the recorded data, i.e., as convolutions with unknown 1-sparse impulse responses. Using this convolutional model, it is possible to formulate a linear system with both the delays and the image of the scene of interest in its nullspace. Furthermore, the 1-sparse structure of the delays and the sparse structure of the scene allow us to restrict the solution space and recover both the relative delay between clocks of pairs of sensors, and the sparse scene. Our numerical simulations verify this intuition and validate our model.

While our work is similar in spirit to our earlier work on position uncertainty in such distributed array systems [11], it demonstrates that small changes in the model—in this particular case timing uncertainty instead of position uncertainty—can result in significantly different final formulations, with different properties and different solution strategies. This is in contrast to most of existing approaches, which simply model the error as a phase error to be recovered, irrespective of whether it is due to timing or position ambiguity. In such approaches, determining the appropriate phase model for each case is particularly difficult, leading to models that do not accurately capture the nature of the errors. Our general optimization-based approach, instead, is able to accurately capture the nature of the error and lead to tractable formulations to obtain the solution.

6. REFERENCES

[1] M. A. Herman and T. Strohmer, "High-resolution radar via compressed sensing," *IEEE transactions on signal processing*, vol. 57, no. 6, pp. 2275–2284, 2009.

[2] Y. Yu, A. P. Petropulu, and H. V. Poor, "Mimo radar using compressive sampling," *IEEE Journal of Selected Topics in Signal Processing*, vol. 4, no. 1, pp. 146–163, 2010.

[3] C. R. Berger and J. M. F. Moura, "Noncoherent compressive sensing with application to distributed radar," in *Information Sciences and Systems (CISS), 2011 45th Annual Conference on*. IEEE, 2011, pp. 1–6.

[4] D. Liu, U. S. Kamilov, and P. T. Boufounos, "Sparsity-driven distributed array imaging," in *Computational Advances in Multi-Sensor Adaptive Processing (CAMSAP), 2015 IEEE 6th International Workshop on*. IEEE, 2015, pp. 441–444.

[5] T Derham, S Doughty, C Baker, and K Woodbridge, "Ambiguity functions for spatially coherent and incoherent multistatic radar," *IEEE Transactions on Aerospace and Electronic Systems*, vol. 46, no. 1, 2010.

[6] W. Ye, T. S. Yeo, and Z. Bao, "Weighted least-squares estimation of phase errors for sar/isar autofocus," *IEEE Transactions on Geoscience and Remote Sensing*, vol. 37, no. 5, pp. 2487–2494, 1999.

[7] Kuang-Hung Liu, Ami Wiesel, and David C Munson, "Synthetic aperture radar autofocus via semidefinite relaxation," *IEEE transactions on image processing*, vol. 22, no. 6, pp. 2317–2326, 2013.

[8] Kuang-Hung Liu, Ami Wiesel, and David C Munson, "Synthetic aperture radar autofocus based on a bilinear model," *IEEE Transactions on image Processing*, vol. 21, no. 5, pp. 2735–2746, 2012.

[9] D. E. Wahl, P. H. Eichel, D. C. Ghiglia, and C. V. Jakowatz, "Phase gradient autofocus-a robust tool for high resolution sar phase correction," *IEEE Transactions on Aerospace and Electronic Systems*, vol. 30, no. 3, pp. 827–835, 1994.

[10] N. O. Onhon and M. Cetin, "A sparsity-driven approach for joint sar imaging and phase error correction," *IEEE Transactions on Image Processing*, vol. 21, no. 4, pp. 2075–2088, 2012.

[11] H. Mansour, D. Liu, P. T. Boufounos, and U. S. Kamilov, "Radar autofocus using sparse blind deconvolution," in *2018 IEEE International Conference on Acoustics, Speech and Signal Processing (ICASSP)*. IEEE, 2018, pp. 1623–1627.

[12] Ali Ahmed, Benjamin Recht, and Justin Romberg, "Blind deconvolution using convex programming," *IEEE Transactions on Information Theory*, vol. 60, no. 3, pp. 1711–1732, 2014.

[13] Yanjun Li, Kiryung Lee, and Yoram Bresler, "Optimal sample complexity for blind gain and phase calibration.," *IEEE Trans. Signal Processing*, vol. 64, no. 21, pp. 5549–5556, 2016.

[14] X. Du, C. Duan, and W. Hu, "Sparse representation based autofocusing technique for isar images," *IEEE Transactions on Geoscience and Remote Sensing*, vol. 51, no. 3, pp. 1826–1835, 2013.

[15] Yanjun Li, Kiryung Lee, and Yoram Bresler, "Identifiability in bilinear inverse problems with applications to subspace or sparsity-constrained blind gain and phase calibration," *IEEE Transactions on Information Theory*, vol. 63, no. 2, pp. 822–842, 2017.

[16] A. Beck and M. Teboulle, "A fast iterative shrinkage-thresholding algorithm for linear inverse problems," *SIAM journal on imaging sciences*, vol. 2, no. 1, pp. 183–202, 2009.

[17] H. J. Cho and D. C. Munson, "Overcoming polar-format issues in multichannel sar autofocus," in *Signals, Systems and Computers, 2008 42nd Asilomar Conference on*. IEEE, 2008, pp. 523–527.

[18] Iain B Collings and Douglas A Gray, "Deconvolution techniques for non-coherent radar images.," in *ISSPA*, 1996, pp. 113–116.